1 **Investigating the Impact of Aerosol Deposition on Snow**

2 **Melt over the Greenland Ice Sheet Using a Large-Ensemble**

3 **Kernel**

4 Yang Li[1], Mark G. Flanner[1]

5 [1] Climate and Space Sciences and Engineering, University of Michigan, Ann Arbor, Michigan, USA

6

7 **Correspondence to:** Y. Li, yanglibj@umich.edu

8

9 **Abstract**

10 Accelerating surface melt on the Greenland Ice Sheet (GrIS) has led to a doubling of

11 Greenland's contribution to global sea level rise during recent decades. Black

12 carbon (BC), dust, and other light absorbing impurities (LAI) darken the surface and

13 enhance snow melt by boosting the absorption of solar energy. It is therefore

14 important for coupled aerosol-climate and ice sheet models to include snow

15 darkening effects from LAI, and yet most do not. In this study, we conduct several

16 thousand simulations with the Community Land Model (CLM) component of the

17 Community Earth System Model (CESM) to characterize changes in melt runoff due

18 to variations in the amount, timing, and nature (wet or dry) of BC deposition on the

19 GrIS. From this large matrix of simulations, we develop a kernel relating runoff to

20 the location, month, year (from 2006-2015), and magnitudes of BC concentration

21 within precipitation and dry deposition flux. BC deposition during June-August

22 causes the largest increase in annually-integrated runoff, but winter deposition

23   events also exert large (roughly half as great) runoff perturbations due to re-

24   exposure of impurities at the snow surface during summer melt. Current BC

25   deposition fluxes simulated with the atmosphere component of CESM induce a

26   climatological-mean increase in GrIS-wide runoff of ~8 Gt/yr, or +6.8% relative to a

27   paired simulation without BC deposition. We also provide linear equations that

28   relate the increase in total runoff to GrIS-wide wet and dry BC deposition fluxes. It

29   is our hope that the runoff kernel and simple equations provided here can be used

30   to extend the utility of state-of-the-art aerosol models.

1 Introduction

The Greenland Ice Sheet (GrIS) holds the equivalent of about 7 m of sea level rise (Kintisch, 2017). During recent decades, the accelerating decline of the GrIS has doubled Greenland's contribution to global sea level rise to about 0.74 mm per year (Shepherd et al., 2012; Rignot and Kanagaratnam, 2006; van den Broeke et al., 2009; Kintisch, 2017). Mass loss from the GrIS is predicted to raise sea level by more than 20 cm by 2100 (Rignot et al., 2011; Dumont et al., 2014), imposing tremendous effects on global society.

Ice loss from the GrIS is caused by many physical and biological factors, including: 1) increase of air temperature over the Arctic region, which accelerates surface melting; 2) declining surface albedo, which can be caused by a variety of effects including increased melt area, enhanced snow metamorphism, and accumulation of light-absorbing impurities (LAI) (Tedesco et al., 2016; Box et al., 2012; Dumont et al., 2014; Keegan et al., 2014; Shimada et al., 2016; Polashenski et al., 2015); and 3) calving of icebergs and submarine melting due to ice dynamics and changes of ocean temperature (Krabill et al., 2004; Zwally et al., 2002; Dumont et al., 2014). Since 2005, surface melting has likely contributed more to ice loss than iceberg calving (Kintisch, 2017). Sources of LAI include black carbon (BC), mineral dust, and algae and bacteria growing on the wet surface of the ice sheet, all of which darken the surface, boost the absorption of insolation and enhance snow melt.

BC is a major anthropogenic pollutant originating from fossil fuel combustion, open biomass burning, and biofuel use, and is a key LAI because its solar

53 absorptivity is extremely high (e.g., Bond et al., 2013). Previous climate modeling

54 studies simulate annual warming in the Arctic region with the inclusion of BC in

55 snow (Flanner et al., 2007; Flanner et al., 2009; Hansen and Nazarenko, 2004;

56 Hansen et al., 2005; Jacobson, 2004), and find BC/snow forcing induces a global

57 temperature response about three times greater than equal forcing from CO_2

58 (Flanner et al., 2007). BC influences snow coverage by warming the atmosphere,

59 reducing surface insolation through "dimming", and reducing snow reflectance

60 through darkening caused by BC deposition to snow surface. Globally, the darkening

61 effect within snow increases solar heating of snowpack, and exceeds the loss of

62 absorbed energy from dimming, causing a positive net surface forcing and

63 snowpack melting (Flanner et al., 2009). Melting snow also tends to retain BC

64 aerosols, which darken the surface more and increase absorption of insolation (e.g.,

65 Doherty et al., 2013). Therefore, it is important for coupled aerosol-climate and ice

66 sheet models to include BC darkening effects, and yet most do not.

67   Global BC emissions from fossil fuel and biofuel combustion have increased

68 dramatically during the industrial era. Since the early 20th century, BC emissions

69 also shifted spatially, decreasing in North American and Europe but increasing in

70 Asia (Bond et al., 2007; Bond et al., 2013). Both the spatial pattern of emissions and

71 the circulation features that are coincident with emissions can strongly effect the

72 amount of BC reaching the Arctic and depositing to the GrIS (Doherty et al., 2010;

73 Thomas et al., 2017; Jiao et al., 2014).

74   In this study, we develop a BC deposition-snow melt kernel using the

75 Community Earth System Model (CESM) to investigate changes in snow melt and

76   surface runoff due to variations in the amount and timing of aerosol deposition on

77   the GrIS. More than 5000 simulations are conducted with the Community Land

78   Model (CLM) component of CESM, driven with a large range of wet and dry BC

79   deposition fluxes to determine relationships between snow melt perturbation and

80   deposition amount occurring in different months. The final kernel product is

81   resolved by type of BC deposition (wet or dry), deposition amount, deposition

82   month, and deposition year ranging from 2006-2015. It is our hope that this kernel

83   will benefit regional and global aerosol modeling communities by allowing them to

84   estimate GrIS snow melt and surface runoff perturbations associated with different

85   aerosol deposition fluxes.

86   **2   Methods**

87   **2.1   Simulation design**

88   We use the Community Earth System Model (CESM) version 1.2.2, and run the

89   offline Community Land Model (CLM) (Oleson et al., 2013) version 4.5 with

90   prescribed wet or dry BC deposition in the snow sub-model to study the effects of

91   BC deposition on snow melt and runoff from Greenland. Our motivation for using

92   CLM in this offline configuration is that (1) it reduces noise associated with ocean

93   and atmosphere variability, enabling clearer identification of the runoff signal

94   caused by snow perturbations, and (2) the simulations are computationally cheap,

95   allowing us to explore a large parameter space. We drive the simulations using

96   meteorological forcing data from the Climatic Research Unit and National Centers

97   for Environmental Prediction (CRUNCEP) (Viovy, 2012) over the period 2006-2016.

98   CRUNCEP data cover the global land surface at a spatial resolution of a $0.5° \times 0.5°$,

99   and are provided with relatively low latency, allowing us to explore conditions over

100   the recent past. In CLM, the representation of terrestrial snow, including over ice

101   sheets, is based loosely on the SNTHERM model (Jordan, 1991) and is described in

102   detail by Oleson et al., 2013. Snow albedo and solar absorption within each snow

103   layer are simulated with the Snow, Ice, and Aerosol Radiative Model (SNICAR),

104   which accounts for solar zenith angle, albedo of the substrate underlying snow,

105   mass concentrations of LAI (black carbon, dust, organic carbon, and volcanic ash),

106   and ice effective grain size. In general, CLM/SNICAR represents five vertical snow

107   layers, and accounts for variations in LAI concentration due to dry and wet

108   deposition, particle flushing and retention with melt water, snow sublimation, and

109   layer combinations and divisions (Oleson et al., 2013). Dry BC deposition from the

110   atmosphere occurs through gravitational settling and turbulent mixing, primarily

111   transferring hydrophobic BC to the surface, while wet BC deposition occurs via

112   precipitation and only affects hydrophilic BC in the model. CLM maintains mass

113   burdens of both hydrophilic BC and hydrophobic BC within each snow layer, with

114   each species having unique optical properties and meltwater removal efficiencies.

115   Deposited particles are assumed to be instantly mixed and homogeneous within the

116   surface snow layer, which does not exceed 2 cm in thickness. The particles are

117   added after the computation of inter-layer water fluxes, thus preventing particles in

118   the top layer from being washed out immediately before radiative calculations.

119   Particle masses are redistributed vertically in each time step proportionately with

120   snow melt through the snow column, scaled by the species-specific melt scavenging

121 efficiency, and snow layer combination and subdivision. The masses carried out

122 with meltwater drainage through the bottom snow layer are permanently lost from

123 the snowpack, and are not maintained within the model (Oleson et al., 2013).

124   For each simulation used to generate the kernel relating melt runoff to BC

125 deposition, we prescribe uniform concentrations of BC within precipitation or

126 uniform dry deposition fluxes over the ice sheet for a period of one month, and

127 quantify perturbations to snow and melt runoff for one year or more following the

128 period of deposition. 23 unique BC concentrations in precipitation (e.g., snow) are

129 prescribed to provide wet BC flux in the CLM. We use a wide range of wet BC

130 concentrations (from 1 ng g^{-1} ~ 500 ng g^{-1}) with logarithmic spacing, aiming to

131 cover historically observed BC concentrations over the Greenland region (Figure 1)

132 and potential severe episodes associated (e.g.,) with extreme fire activity. For

133 example, measured values of BC in Greenland snow during 2012-2014, collected

134 from snow pits across a long transect, averaged 2.6 ng g^{-1} (Polashenski et al.,

135 2015). Peak values throughout the depth of the snow pits averaged 4 ng g^{-1} and 15

136 ng g^{-1} in 2012 and 2013, respectively, and the largest single measurement was 43 ng

137 g^{-1}. Ice core measurements from D4 dating back to 1788 show annual-mean

138 concentrations peaking in the early 20th century at ~12.5 ng g^{-1}, mean

139 concentrations of 2.3 ng g^{-1} during 1952-2002, and occasional monthly-mean peaks

140 exceeding 50 ng g^{-1} due to biomass burning events (McConnell et al., 2007).

141 Correspondingly, the maximum dry BC deposition flux is calculated as the product

142 of the maximum wet BC concentration (500 ng g^{-1}) and the mean monthly snowfall

143 (1.75×10^{-5} mm s^{-1}) over an 11-year (2006-2016) CESM simulation. We prescribe 24

144   unique dry BC fluxes (0.01 ng m^{-2} s^{-1}-8.80 ng m^{-2} s^{-1}) with logarithmic spacing in our

145   study (Figure 1).

146   With each prescribed BC deposition value, we perform 12 simulations with

147   specified BC deposition month from January to December in each deposition year.

148   Each simulation starts from January in the deposition year, and extends to one full

149   year after the deposition month in order to study the annually integrated BC effects.

150   We then repeat these simulations for ten years (2006-2015) to generate a

151   climatological product and explore the magnitude of interannual variability in melt

152   perturbations due, for example, to differences in precipitation and near-surface air

153   temperatures. In summary, we perform 2,760 simulations (23 wet BC

154   concentrations × 12 deposition months × 10 deposition years) to study the effects of

155   wet BC deposition, and 2,880 simulations (24 dry BC fluxes × 12 deposition months

156   × 10 deposition years) to study the effects of dry BC deposition. 120 simulations (12

157   deposition months × 10 deposition years) without BC deposition are also performed

158   as parallel control/base runs from which to derive the perturbations induced by BC

159   deposition. The timestep of CLM/SNICAR for our simulations is 0.5 hour, and the

160   spatial resolution is 0.9° x 1.25°. The kernel product is calculated as monthly mean

161   values with the same spatial resolution.

162   **2.2   Simulation length evaluation based on top-snow layer BC concentration**

163   To evaluate the importance of simulation length for the purposes outlined, we

164   focus on BC concentration in the top snow layer because properties of this layer

165   dominate the bulk solar radiative properties of the snowpack. In Figure 2, we

166   examine the mean distribution of BC concentration in the top snow layer over

167   Greenland after maximum wet and dry BC deposition fluxes occur in January and

168   June. These contours are averaged over ten years to show a climatological state.

169   Top-layer BC concentrations after wet BC deposition show higher values in the

170   center and south margin of Greenland (Figure 2a, b, e, f), which matches the general

171   precipitation pattern over the GrIS, with elevated precipitation amount in the center

172   and south of GrIS. Meanwhile, higher top-layer BC values occur over the north of

173   Greenland after dry BC deposition (Figure 2c, d, g, h), as lower precipitation in these

174   regions enhances the effect of dry deposition. Also, we find lower concentrations

175   induced by the maximum wet BC (Figure 2a, b, e, f) than by the maximum dry BC

176   deposition (Figure 2c, d, g, h). Top-layer BC concentration decreases rapidly only

177   one month after the deposition month for both winter and summer deposition (i.e.,

178   from January to February with January deposition in Figure 2a-d, and from June to

179   July with June deposition in Figure 2e-h), as new snowfall dilutes the contaminated

180   snow. The rapid decrease in BC concentration supports the notion that a one-year

181   simulation length should capture most of the time-integrated effect from a

182   deposition event. To verify this, we also perform two 11-year (2006-2016)

183   simulations with the maximum wet BC deposition occurring in April and October of

184   the first year, to evaluate the long-term variation of top-layer BC concentration. In

185   these long-term simulations, we find top-layer BC concentrations decrease rapidly

186   within a one-year period after both spring and fall depositions (Figure 3). We also

187   see, however, that residual BC reappears at the surface in subsequent summers

188   because of snow melting and associated accumulation of impurities at the top of the

189   snowpack (Doherty et al., 2013). In the model, this occurs because melt scavenging

190   ratios for both types of BC are less than 1, meaning that proportionately less BC

191   moves down vertically in the column than meltwater. As we will see, summer re-

192   appearance of impurities at the snow top has a non-negligible impact on the

193   annually-integrated runoff perturbation, but the peaks in subsequent years are less

194   than 1/20 of the BC concentrations in the deposition month, indicating that the one-

195   year simulation setup is reasonable to capture the major portion of the total BC

196   influences.

197   **3   Results and Discussion**

198   Deposited BC to snow causes a darkening effect and enhances snow melt and

199   Greenland runoff. Here, we first show variations of top-snow layer BC

200   concentrations, and then examine total GrIS runoff perturbation induced by BC

201   deposition.

202   **3.1   BC concentration in the top snow layer**

203   We investigate the climatological (i.e., averaged over ten simulations covering

204   2006-2015) 1-year evolution of top-snow layer BC concentration averaged over

205   Greenland for different deposition months. Figure 4 depicts the temporal evolution

206   of top-layer BC concentration for the maximum wet and dry BC fluxes from our

207   matrix of simulations. For all months of deposition, top-layer concentrations

208   decrease rapidly as fresh snow covers the contaminated surface. Top-snow layer

209   concentrations of dry-deposited BC generally decrease more slowly than those of

210   wet-deposited BC. One reason for this behavior during summer months is that dry-

211   deposited BC is assumed to be hydrophobic and have a lower meltwater scavenging

212 efficiency, reducing the rate at which it is carried away by melting water. We also

213 see, however, that some winter-deposited BC can persist in the top layer until, or

214 even re-appear during, the summer melt season, indicating that BC deposition in

215 non-melting seasons can also be important for GrIS melting. Re-exposure of

216 previously deposited BC occurs as overlying snow melts and flushes through the

217 snow, removing some but not all of the underlying impurities and eventually

218 exposing the dirty snow layer at the surface.

219   We also investigate how top-layer BC concentration varies with different BC

220 deposition values, and how this variation evolves over one year following

221 deposition (Figure 5 and Figure 6). For all deposition months, top-snow layer BC

222 concentration increases, as expected, with increasing BC deposition flux. The

223 relationship between top-layer BC concentration and BC deposition value is nearly

224 linear, although we find indications of saturation at later times with dry BC

225 deposition (e.g., as in Figure 6h-l). Figure 7 summarizes top-layer BC concentration

226 variation with deposition amount at different times (0-11 months since deposition)

227 averaged over all the deposition months. With this averaging, we find that top-layer

228 BC concentrations decrease monotonically from month 0 to month 11. Again, we

229 find slower decrease in the dry deposition simulations than in the wet deposition

230 simulations. With wet BC deposition, the rate of decrease slows down after 3-6

231 months, which could be due to the summer peaks resulting from snow melting and

232 BC integration (Figure 4).

233 **3.2   Temporal variation of GrIS total runoff**

234   We define total runoff in CLM as the summation of surface runoff, sub-surface

11

235 drainage and runoff from glacier surface. We first examine the seasonal and inter-

236 annual variation of GrIS total runoff, integrated over the entire GrIS, in the base run

237 without BC deposition (Figure 8). Total runoff shows clear summer peaks and some

238 inter-annual variation. Annual-integrated total runoff is ~120 Gt per year, with the

239 highest value of ~140 Gt in 2014 (Figure 8b). Compared with satellite gravity

240 measurements during 2005-2010 showing Greenland is losing mass at a rate of

241 ~229 Gt/yr (169-290 Gt/yr), of which 50-70% is lost through surface melt

242 (Vaughan et al., 2013), the simulated total runoff in the base run in our study is

243 within a reasonable range.

244   We then calculate perturbed total runoff due to BC deposition as the difference

245 in runoff between simulations with BC deposition and paired base simulations

246 without BC deposition. We select three wet BC deposition values and three dry BC

247 deposition values to illustrate the seasonal and inter-annual variations of perturbed

248 total runoff (Figure 9). We note that different scales are used in the panels of Figure

249 9, which shows that higher deposition causes more total runoff. We also find clear

250 inter-annual variations for different deposition amounts and months. The variations

251 of perturbed total runoff in Figure 9 follow the variation of total runoff in the base

252 run (Figure 8) in general, especially for the perturbed simulations with wet BC

253 depositions, indicating that BC deposition could have greater effect in warmer years,

254 when more of the ice sheet is near the melting temperature. This could also be due

255 to an amplification effect by metamorphism of snow in warmer years.

256   To remove the effect of yearly variation, we also investigate the climatological

257 (i.e., averaged over ten simulations spanning 2006-2015) 1-year evolution of total

258   runoff increase due to BC deposition starting from different deposition months.

259   Again, we examine total runoff increase induced by maximum wet and dry BC

260   depositions to understand general behavior associated with very large

261   perturbations, for which the signal is much larger than noise. As shown in Figure

262   10, we find two summer peaks of total runoff increase, with the second peak caused

263   by the re-exposure of BC during the summer after deposition. We also find total

264   runoff perturbation is the largest in July for all months of deposition, followed by

265   August. The largest perturbation in summer could be caused by immediate melting

266   due to darkening, as well as larger grain size in warmer environment.

267   **3.3   GrIS total runoff variation with deposition amount**

268   As represented by Figure 9, higher deposition amount causes larger total runoff

269   increase. Here, we examine total runoff perturbation caused by all deposition

270   amounts, and how total runoff distributes over Greenland. Figure 11 and Figure 12

271   show climatological mean (2006-2015) annually integrated total runoff increase

272   caused by June BC deposition via wet and dry processes, respectively. June

273   deposition is selected for these figures because of its high potential to impact

274   summer melt. Although BC is well distributed over the whole GrIS (Figure 2), total

275   runoff perturbations are largely confined to the low elevation margins with both

276   wet and dry BC deposition (Figure 11 and Figure 12), as these remain the only areas

277   warm enough in the model simulations for substantial melt to occur, which is

278   consistent with the Tedesco, 2007 study. We note that the spatial distribution of

279   model melt will be sensitive to surface air temperature and insolation, the latter of

280   which can vary substantially between re-analysis products. Runoff effects of dry BC

281 deposition show similar patterns as impacts from BC in precipitation. We find that

282 small fluxes of BC via dry deposition are not as effective as similar deposition fluxes

283 of BC in precipitation, and we attribute this to the higher light absorptivity (and

284 hence radiative forcing per unit mass) of hydrophilic BC than of hydrophobic BC.

285 The former is assumed to be coated with non-absorbing sulfate and hence its mass

286 absorption cross-section is about 50% larger than that of uncoated hydrophobic BC

287 (Flanner et al., 2007).

288   Figure 13 summarizes the variation of total runoff perturbation versus

289 deposition amount for different deposition months. The maximum BC deposition

290 perturbs total runoff by up to ~20% (24 Gt) in the wet BC deposition simulations,

291 although we note that continent-wide fluxes of this magnitude (500 ng g^{-1} in

292 precipitation) are much larger than ever observed on Greenland. With a modest

293 deposition concentration (e.g., 5 ng/g), the runoff perturbation is ~0.4% (~0.5 Gt).

294 Different deposition months cause annually integrated total runoff perturbation to

295 vary by 40-60% (12 Gt/yr in the maximum BC deposition case). Also, we find BC

296 deposition in June and July induces the largest annually integrated total runoff

297 increase. To further verify the most influential deposition month, we select five wet

298 BC and five dry BC deposition values, and plot total runoff increase versus

299 deposition month, shown in Figure 14. Figure 14a shows annual integrated total

300 runoff from the base run, starting from different months, serving as a reference for

301 the perturbations shown in Figure 14b-f. For different deposition amounts from low

302 to high (Figure 14b-f), BC deposition in summer (i.e., June, July and August) causes

303 the highest annual total runoff increase. With higher deposition (Figure 14e-f), June

14

304 deposition generates the largest annual total runoff for both dry and wet BC

305 deposition, whereas with lower deposition amounts the month of maximum impact

306 can be June or July. As noted earlier, however, deposition during non-summer

307 months also causes substantial melt and runoff perturbations, owing to the melt-

308 induced re-surfacing of impurities during summer in the ablation zone.

309 **4   Evaluation and application of the kernel product**

310   We turn now to evaluating the kernel product and advising a straightforward

311 way in which it can be applied to realistic aerosol deposition fluxes. We perform ten

312 one-year CLM simulations with spatially and temporally-varying wet or dry BC

313 deposition fluxes occurring in randomly selected years and months, and we evaluate

314 the accuracy of the kernel product using total GrIS BC deposition amount and total

315 runoff from these new simulations (the "evaluating simulations"), compared with

316 total runoff from the kernel for equivalent deposition fluxes. The evaluating

317 simulations use prescribed wet and dry BC deposition fields that were generated

318 from a global aerosol run with CAM (Lamarque et al., 2010). In different evaluating

319 simulations, the prescribed BC deposition fields are multiplied by factors ranging

320 from 2-50 for wet BC deposition and 2000-20000 for dry BC deposition to provide

321 different BC deposition amounts within the range of wet or dry deposition in the

322 kernel. High scaling factors are applied to dry/hydrophobic BC deposition

323 simulations because the prescribed dry BC deposition from CAM is very low and

324 within the noise regime. We also perform two ten-year (2006-2015) evaluating

325 simulations with both CAM prescribed wet and dry BC deposition fluxes turned on

326   throughout the whole simulations, to examine short-term, long-term and

327   climatological one-year integrated total runoff effects. BC deposition fluxes in one of

328   the ten-year evaluating simulations are multiplied by a factor of 5 to provide a high

329   deposition event and are left at unperturbed (i.e., realistic) values in the other

330   simulation. Also, different deposition years and months indicate different BC

331   distributions. Therefore, the evaluating simulations provide a variety of scenarios

332   with distinct BC deposition amounts and distributions to evaluate performance of

333   the kernel.

334   Figure 15 shows maximum, mean and minimum one-year integrated total

335   runoff increase versus BC deposition amount from the kernel product, with results

336   from the evaluating simulations overlaid on the kernel lines. With varying BC

337   deposition amount and distribution, including with combined wet and dry BC

338   deposition fluxes, results from the evaluating simulations are mostly within the total

339   runoff ranges of our kernel product for both wet and dry BC deposition. In the

340   evaluating simulations with combined wet and dry BC depositions, hydrophobic BC

341   fluxes are very low (<1/100 of wet BC fluxes), therefore, we treat all BC deposition

342   as wet/hydrophilic BC, and overlay the results on the wet deposition curves. We

343   note CAM simulated BC deposition from the 1 time evaluating run is comparable

344   with measured values of BC in Greenland snow and ice core measurements

345   (Polashenski et al., 2015; McConnell et al., 2007). The increases of one-year

346   integrated total runoff from the ten-year evaluating simulations with realistic

347   deposition exhibit wide ranges, for example, with a minimum of ~4 Gt in the first

348   deposition year (2006) to a maximum of ~10 Gt, and with a minimum of ~14 Gt in

349   the first year to a maximum of ~40 Gt in the simulation with 5 times BC fluxes. The

350   climatological (i.e., averaged over 10 years) total runoff perturbations (~8 Gt/yr and

351   ~30 Gt/yr in the default and 5 times simulations, respectively) caused by prescribed

352   combined wet and dry BC deposition are about double the first-year total runoff

353   integrations, which is due to continuous month by month depositions in the ten-

354   year evaluating simulations and the long-term effects of the reappearance of

355   residual BC at the surface as described in section 2.2.

356   Because the mean and maximum kernel curves in Figure 15 provide estimates

357   of BC induced total runoff within a reasonable range, we parameterize these curves

358   to provide a simple application of our kernel product. GrIS-wide melt perturbations

359   are relatively linear with BC deposition amount, with linear fits to the mean kernel

360   curves for wet and dry BC deposition fluxes of, respectively:

361       $\Delta TOTALRUNOFF = 4.498e5 * \Delta wetBC,$ (1)

362       $\Delta TOTALRUNOFF = 3.062e5 * \Delta dryBC,$ (2)

363   and with linear fits to the maximum kernel curves of:

364       $\Delta TOTALRUNOFF\_MAX = 9.322e5 * \Delta wetBC,$ (3)

365       $\Delta TOTALRUNOFF\_MAX = 6.348e5 * \Delta dryBC,$ (4)

366   where $\Delta TOTALRUNOFF$ is the mean increase in one-year integrated total runoff (kg

367   yr^{-1}), $\Delta TOTALRUNOFF\_MAX$ is the maximum increase in one-year integrated total

368   runoff (kg yr^{-1}), and $\Delta wetBC$ and $\Delta dryBC$ are total wet and dry BC deposition fluxes

369   to the GrIS (kg yr^{-1}). Unique relationships for wet and dry deposition arise, again,

370   because of differences in optical properties and melt-induced removal efficiencies of

371   hydrophilic and hydrophobic BC. Linearity in the relationship between runoff and

372   BC deposition is encouraging because we have neglected coincident darkening from

373   other types of LAI (e.g., dust, algae). In environments where darkening from other

374   LAI is not too great, the runoff–BC relationships derived here should be valid,

375   though we acknowledge that the incremental effect of BC will be lower in snow that

376   is heavily laden with other impurities.

377   The bulk relationships shown above represent the simplest application of our

378   kernel product, allowing a rough estimation of runoff perturbation caused by

379   Greenland-wide wet and dry BC deposition fluxes. Based on the evaluations in

380   Figure 15, the mean curves (i.e., equations (1) and (2)) from the kernel product tend

381   to provide a conservative estimate of total runoff, whereas the maximum curves

382   (i.e., equations (3) and (4)) represent a more realistic approximation of total runoff

383   induced by BC deposition that occurs continuously and with varying spatial

384   distribution. Ideally, gridcell-by-gridcell fluxes should be matched to the kernel to

385   account for spatial differences in melt associated with elevation and other

386   conditions (Figure 11 and Figure 12), but at the low end of deposition flux we see

387   considerable noise at the individual pixel and deposition month level, especially for

388   wet deposition fluxes that can be subject to anomalies associated with low

389   precipitation amounts in a given month. To ameliorate this, for typical present-day

390   deposition fluxes we recommend matching month-specific, but spatially-integrated

391   deposition fluxes or concentrations with the associated Greenland-wide kernel

392   values.

393   Finally, although this product only includes BC, we suggest that it could be

394   extended to include other LAI species through a simple scaling that accounts for the

395 ratio of mass-specific absorption between the species of interest and the BC

396 explored here. Rationale for this is that radiative forcing and melt perturbation will

397 scale roughly linearly with absorptivity, at least for relatively low and moderate

398 burdens of LAI. The mass-specific visible band absorption cross-sections assumed

399 in our study for hydrophilic (via wet deposition) and hydrophobic (via dry

400 deposition) BC are 7.5 and 11.3 $m^2\,g^{-1}$, respectively. The only other species-specific

401 property affecting results from this study is the meltwater scavenging coefficient,

402 which is assumed to be 0.2 for hydrophilic BC and 0.03 for hydrophobic BC (Flanner

403 et al., 2007). Given relatively large uncertainty in this parameter (Doherty et al.,

404 2013; Qian et al., 2014), we suggest applying the hydrophilic (wet deposition)

405 kernel to all hydrophilic species and the hydrophobic (dry deposition) kernel to all

406 hydrophobic species, along with appropriate scaling of optical properties.

407 **5   Conclusions**

408   In this study, ~6,000 simulations are performed to investigate annually

409 integrated runoff perturbation from BC deposition on snow. The simulation matrix

410 includes variations in deposition flux, deposition month and year, and nature of the

411 deposition (wet or dry). From this matrix we produce a large-ensemble kernel that

412 relates BC deposition fluxes to GrIS runoff perturbations.

413   In the month after deposition, top-snow layer BC concentration decreases

414 rapidly due to fresh snow coverage, but then increases somewhat in the ablation

415 zone during the following summer due to melt-induced re-exposure of the

416 contaminated snow. Accordingly, the total runoff increase induced by BC deposition

417   is substantial for both summer and winter deposition, though with peak impacts

418   associated with June and July deposition. Impacts from winter deposition suggest

419   that winter emissions, associated for example with biomass heating use, should not

420   be neglected as potential contributors to increased summer melt. Also, we find most

421   of the runoff increase occurs along the margins, and especially on the southern

422   margin of Greenland, with little sign of melting in the center of the GrIS where it is

423   rarely warm enough. Inter-annual variations in total runoff in the base and BC

424   perturbed simulations indicate that BC deposition can generate more impact in

425   warmer years, when more of the ice surface is near the melting temperature.

426   In summary, higher BC deposition amount leads to higher total runoff. We do

427   not find a clear sign of runoff saturation caused by high BC deposition values in our

428   study. Model-generated deposition fluxes associated with realistic BC emissions

429   induce a climatological-mean (2006-2015) GrIS-wide runoff increase of 8 Gt/yr

430   (+6.8% perturbation), which corresponds to 0.022 mm/year of global sea level rise.

431   We also suggest simple, linear equations that crudely relate GrIS-wide wet and dry

432   BC deposition fluxes to annually-integrated runoff perturbation, and provide links

433   to the full spatially-varying kernel dataset so that users can derive more accurate

434   estimates of melt perturbation (e.g., resolved by seasonal timing) from deposition

435   fluxes. We also suggest that the kernel results can be applied to other LAI species

436   via simple scaling of the mass absorption cross-section. Our hope is that these data

437   will extend the utility of state-of-the-art aerosol models.

438

Acknowledgments

References

Bond, T. C., Bhardwaj, E., Dong, R., Jogani, R., Jung, S., Roden, C., Streets, D. G., and Trautmann, N. M.: Historical emissions of black and organic carbon aerosol from energy-related combustion, 1850–2000, Global Biogeochemical Cycles, 21, n/a-n/a, 10.1029/2006GB002840, 2007.

Bond, T. C., Doherty, S. J., Fahey, D. W., Forster, P. M., Berntsen, T., DeAngelo, B. J., Flanner, M. G., Ghan, S., Kärcher, B., Koch, D., Kinne, S., Kondo, Y., Quinn, P. K., Sarofim, M. C., Schultz, M. G., Schulz, M., Venkataraman, C., Zhang, H., Zhang, S., Bellouin, N., Guttikunda, S. K., Hopke, P. K., Jacobson, M. Z., Kaiser, J. W., Klimont, Z., Lohmann, U., Schwarz, J. P., Shindell, D., Storelvmo, T., Warren, S. G., and Zender, C. S.: Bounding the role of black carbon in the climate system: A scientific assessment, Journal of Geophysical Research: Atmospheres, 118, 5380-5552, 10.1002/jgrd.50171, 2013.

Box, J., Fettweis, X., Stroeve, J., Tedesco, M., Hall, D., and Steffen, K.: Greenland ice sheet albedo feedback: thermodynamics and atmospheric drivers, The Cryosphere, 6, 821-839, 2012.

Doherty, S., Warren, S., Grenfell, T., Clarke, A., and Brandt, R.: Light-absorbing impurities in Arctic snow, Atmospheric Chemistry and Physics, 10, 11647-11680, 2010.

Doherty, S. J., Grenfell, T. C., Forsström, S., Hegg, D. L., Brandt, R. E., and Warren, S. G.: Observed vertical redistribution of black carbon and other insoluble light‐absorbing particles in melting snow, Journal of Geophysical Research: Atmospheres, 118, 5553-5569, 2013.

Dumont, M., Brun, E., Picard, G., Michou, M., Libois, Q., Petit, J. R., Geyer, M., Morin, S., and Josse, B.: Contribution of light-absorbing impurities in snow to Greenland's darkening since 2009, Nature Geoscience, 7, 509, 10.1038/ngeo2180 https://www.nature.com/articles/ngeo2180#supplementary-information, 2014.

Flanner, M. G., Zender, C. S., Randerson, J. T., and Rasch, P. J.: Present-day climate forcing and response from black carbon in snow, Journal of Geophysical Research: Atmospheres, 112, n/a-n/a, 10.1029/2006JD008003, 2007.

Flanner, M. G., Zender, C. S., Hess, P. G., Mahowald, N. M., Painter, T. H., Ramanathan, V., and Rasch, P.: Springtime warming and reduced snow cover from carbonaceous particles, Atmospheric Chemistry and Physics, 9, 2481-2497, 2009.

Hansen, J., and Nazarenko, L.: Soot climate forcing via snow and ice albedos, Proceedings of the National Academy of Sciences of the United States of America, 101, 423-428, 2004.

Hansen, J. e., Sato, M., Ruedy, R., Nazarenko, L., Lacis, A., Schmidt, G., Russell, G., Aleinov, I., Bauer, M., and Bauer, S.: Efficacy of climate forcings, Journal of Geophysical Research: Atmospheres, 110, 2005.

485   Jacobson, M. Z.: Climate response of fossil fuel and biofuel soot, accounting for soot's
486   feedback to snow and sea ice albedo and emissivity, Journal of Geophysical
487   Research: Atmospheres, 109, 2004.
488   Jiao, C., Flanner, M., Balkanski, Y., Bauer, S., Bellouin, N., Berntsen, T., Bian, H.,
489   Carslaw, K., Chin, M., and De Luca, N.: An AeroCom assessment of black carbon in
490   Arctic snow and sea ice, Atmospheric Chemistry and Physics, 14, 2399-2417,
491   2014.
492   Jordan, R.: A one-dimensional temperature model for a snow cover: Technical
493   documentation for SNTHERM. 89, COLD REGIONS RESEARCH AND ENGINEERING
494   LAB HANOVER NH, 1991.
495   Keegan, K. M., Albert, M. R., McConnell, J. R., and Baker, I.: Climate change and forest
496   fires synergistically drive widespread melt events of the Greenland Ice Sheet,
497   Proceedings of the National Academy of Sciences, 111, 7964-7967, 2014.
498   Kintisch, E.: Meltdown, in, American Association for the Advancement of Science,
499   2017.
500   Krabill, W., Hanna, E., Huybrechts, P., Abdalati, W., Cappelen, J., Csatho, B., Frederick,
501   E., Manizade, S., Martin, C., and Sonntag, J.: Greenland ice sheet: increased coastal
502   thinning, Geophysical Research Letters, 31, 2004.
503   Lamarque, J.-F., Bond, T. C., Eyring, V., Granier, C., Heil, A., Klimont, Z., Lee, D.,
504   Liousse, C., Mieville, A., and Owen, B.: Historical (1850–2000) gridded
505   anthropogenic and biomass burning emissions of reactive gases and aerosols:
506   methodology and application, Atmospheric Chemistry and Physics, 10, 7017-
507   7039, 2010.
508   McConnell, J. R., Edwards, R., Kok, G. L., Flanner, M. G., Zender, C. S., Saltzman, E. S.,
509   Banta, J. R., Pasteris, D. R., Carter, M. M., and Kahl, J. D.: 20th-century industrial
510   black carbon emissions altered arctic climate forcing, Science, 317, 1381-1384,
511   2007.
512   Oleson, K., Lawrence, M., Bonan, B., Drewniak, B., Huang, M., Koven, D., Levis, S., Li, F.,
513   Riley, J., and Subin, M.: Technical description of version 4.5 of the Community
514   Land Model (CLM), 2013.
515   Polashenski, C. M., Dibb, J. E., Flanner, M. G., Chen, J. Y., Courville, Z. R., Lai, A. M.,
516   Schauer, J. J., Shafer, M. M., and Bergin, M.: Neither dust nor black carbon causing
517   apparent albedo decline in Greenland's dry snow zone: Implications for MODIS
518   C5 surface reflectance, Geophysical Research Letters, 42, 9319-9327, 2015.
519   Qian, Y., Wang, H., Zhang, R., Flanner, M. G., and Rasch, P. J.: A sensitivity study on
520   modeling black carbon in snow and its radiative forcing over the Arctic and
521   Northern China, Environmental Research Letters, 9, 064001, 2014.
522   Rignot, E., and Kanagaratnam, P.: Changes in the velocity structure of the Greenland
523   Ice Sheet, Science, 311, 986-990, 2006.
524   Rignot, E., Velicogna, I., van den Broeke, M. R., Monaghan, A., and Lenaerts, J. T.:
525   Acceleration of the contribution of the Greenland and Antarctic ice sheets to sea
526   level rise, Geophysical Research Letters, 38, 2011.
527   Shepherd, A., Ivins, E. R., Geruo, A., Barletta, V. R., Bentley, M. J., Bettadpur, S., Briggs,
528   K. H., Bromwich, D. H., Forsberg, R., and Galin, N.: A reconciled estimate of ice-
529   sheet mass balance, Science, 338, 1183-1189, 2012.

530 Shimada, R., Takeuchi, N., and Aoki, T.: Inter-annual and geographical variations in
531   the extent of bare ice and dark ice on the Greenland ice sheet derived from MODIS
532   satellite images, Frontiers in Earth Science, 4, 43, 2016.
533 Tedesco, M.: Snowmelt detection over the Greenland ice sheet from SSM/I
534   brightness temperature daily variations, Geophysical Research Letters, 34, 2007.
535 Tedesco, M., Doherty, S., Fettweis, X., Alexander, P., Jeyaratnam, J., and Stroeve, J.:
536   The darkening of the Greenland ice sheet: trends, drivers, and projections (1981–
537   2100), Cryosphere (The), 10, 477-496, 2016.
538 Thomas, J. L., Polashenski, C. M., Soja, A. J., Marelle, L., Casey, K., Choi, H. D., Raut, J. C.,
539   Wiedinmyer, C., Emmons, L. K., and Fast, J.: Quantifying black carbon deposition
540   over the Greenland ice sheet from forest fires in Canada, Geophysical Research
541   Letters, 2017.
542 van den Broeke, M., Bamber, J., Ettema, J., Rignot, E., Schrama, E., van de Berg, W. J.,
543   van Meijgaard, E., Velicogna, I., and Wouters, B.: Partitioning recent Greenland
544   mass loss, science, 326, 984-986, 2009.
545 Vaughan, D. G., Comiso, J. C., Allison, I., Carrasco, J., Kaser, G., Kwok, R., Mote, P.,
546   Murray, T., Paul, F., and Ren, J.: Observations: cryosphere, Climate change, 2103,
547   317-382, 2013.
548 Viovy, N.: CRU-NCEP Version 4, available at:
549   http://dods.extra.cea.fr/data/p529viov/cruncep/V4_1901_2012/ last access:
550   August 2012.
551 Zwally, H. J., Abdalati, W., Herring, T., Larson, K., Saba, J., and Steffen, K.: Surface
552   melt-induced acceleration of Greenland ice-sheet flow, Science, 297, 218-222,
553   2002.
554

Figure Captions
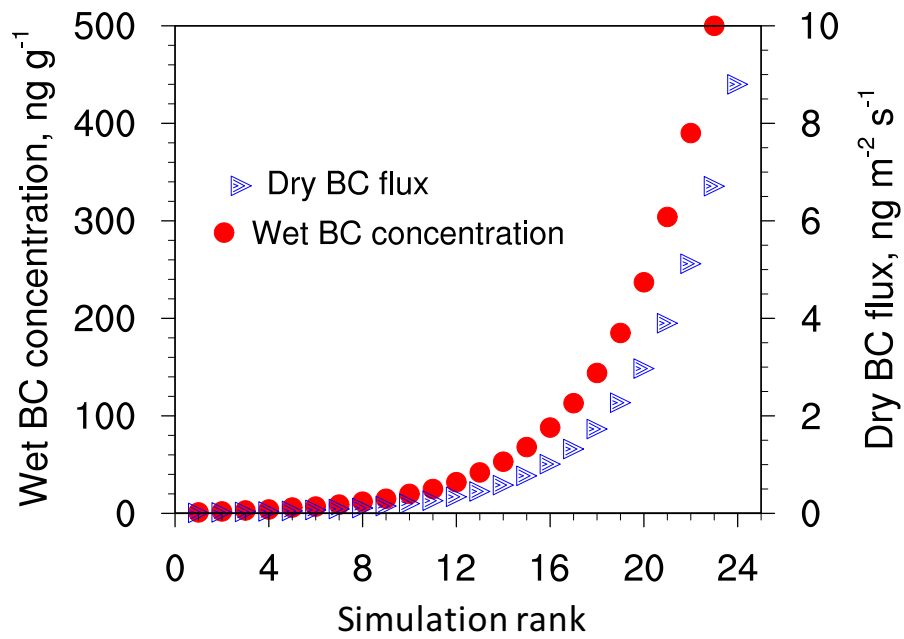
Figure 1. Prescribed values of BC concentrations in precipitation (red) and dry

deposition fluxes (blue) applied in the CESM modeling studies. Spacing between

values is logarithmic.

Wet BC   Dry BC

a) Deposition in January — Jan

b) Feb

c) Jan

d) Feb

e) Deposition in June — Jun

f) Jul

g) Jun

h) Jul

ng g^{-1}

0   200   400   600   800   1000   1200

0   400   800   1500   1900   3500   5500
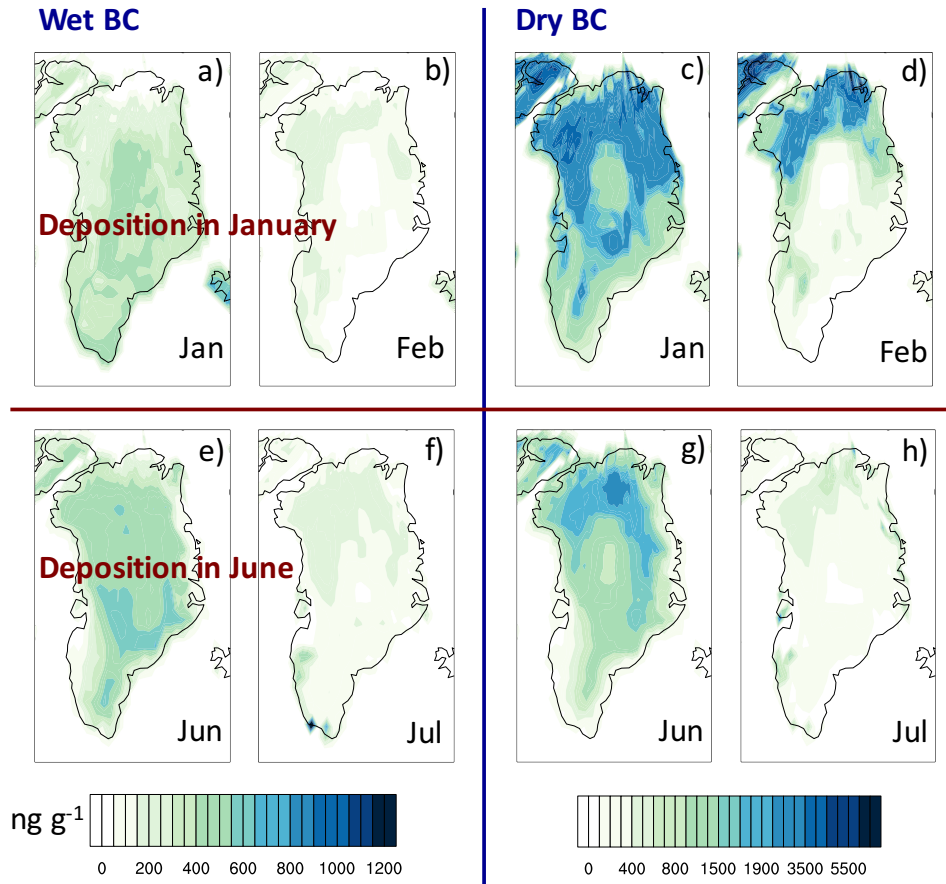
Figure 2. Ten-year (2006-2015) averaged hydrophilic BC concentration associated with wet deposition (a, b, e, f) and hydrophobic BC concentration associated with dry deposition (c, d, g, h) in the top snow layer. The contour maps show concentrations caused by January deposition (a-d) and June deposition (e-h), associated with the maximum wet and dry deposition scenarios depicted in Figure 1.

570
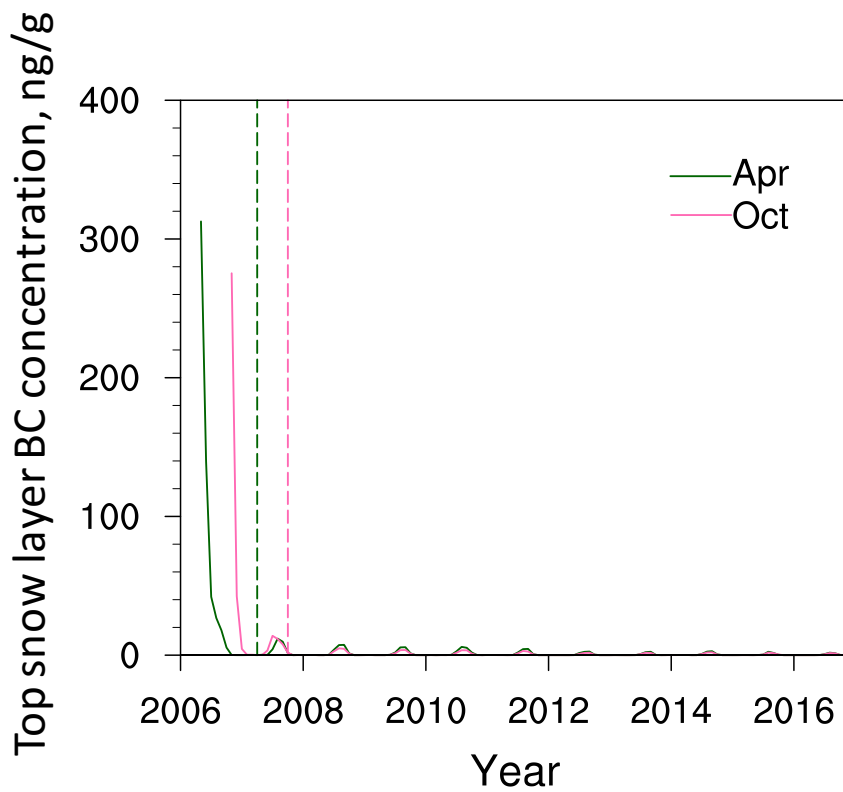
Figure 3. Temporal evolution of hydrophilic BC concentration in the top snow layer

averaged over the Greenland region from two 11-year (2006-2016) simulations

with wet BC deposition occurring in April and October of the first year. The BC

concentration in precipitation is the maximum value shown in Figure 1. Dashed

lines represent the ends of one year since different deposition months.

576

577
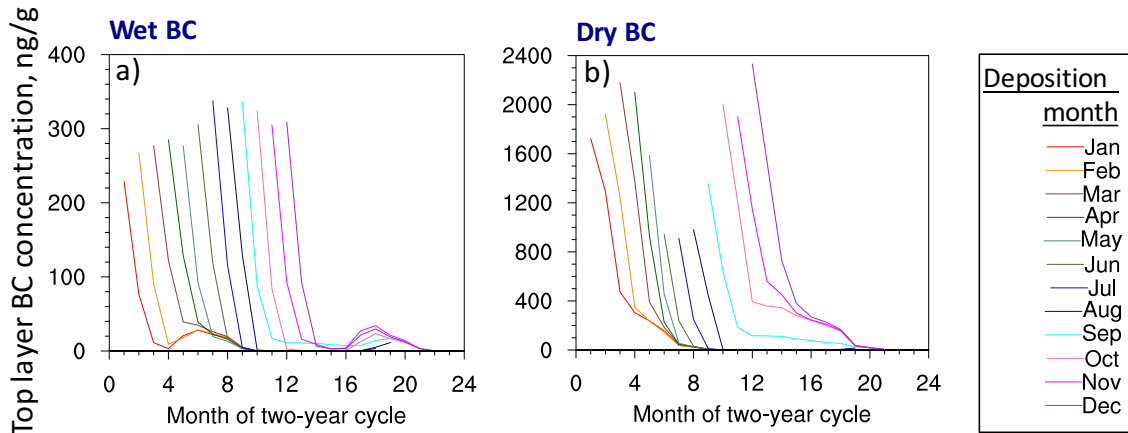
Figure 4. Temporal evolution of hydrophilic BC concentration (a) and hydrophobic

BC concentration (b) in the top snow layer averaged over the Greenland region from

the simulations with the maximum wet and dry BC deposition, respectively. Each

line starts from the BC deposition month, extends one year, and represents the

mean time series from 10 simulations that start in each year from 2006-2015.

583

584
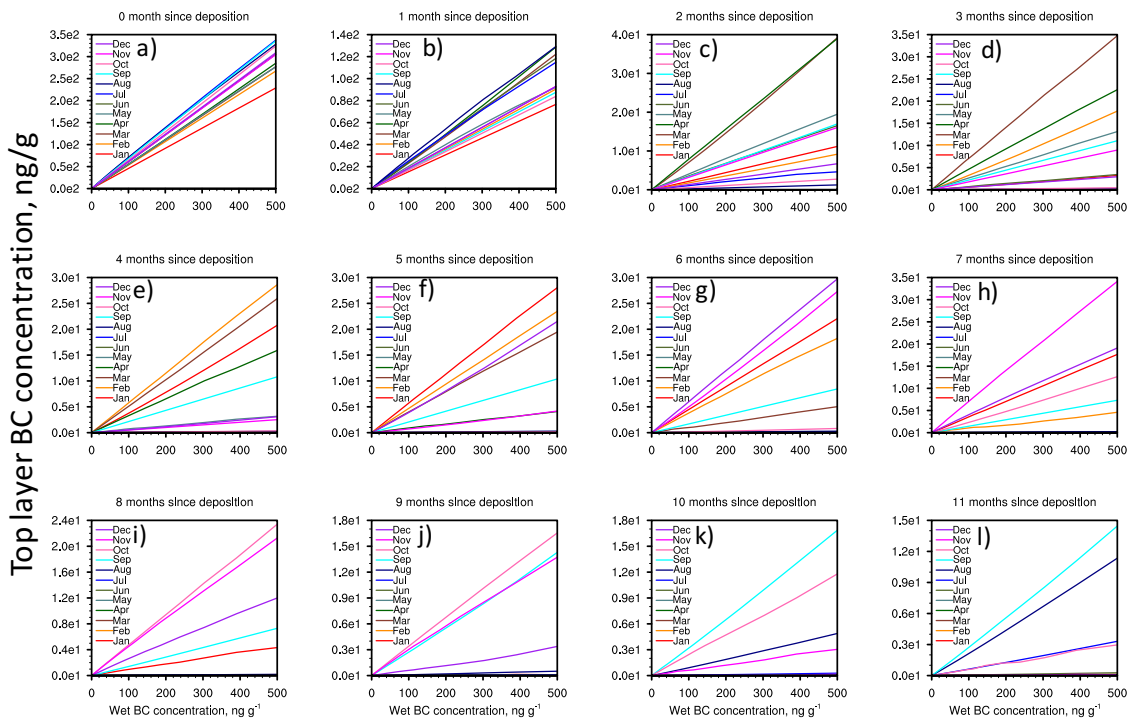
Figure 5. Hydrophilic BC concentration in the top snow layer vs. concentration of

BC in precipitation shown at different times (0-11 months, panels a-l) since

deposition. The top-snow layer concentrations are averaged over the Greenland

region and over ten one-year simulations beginning in years 2006-2015. Different

line colors represent different deposition months.

590

591
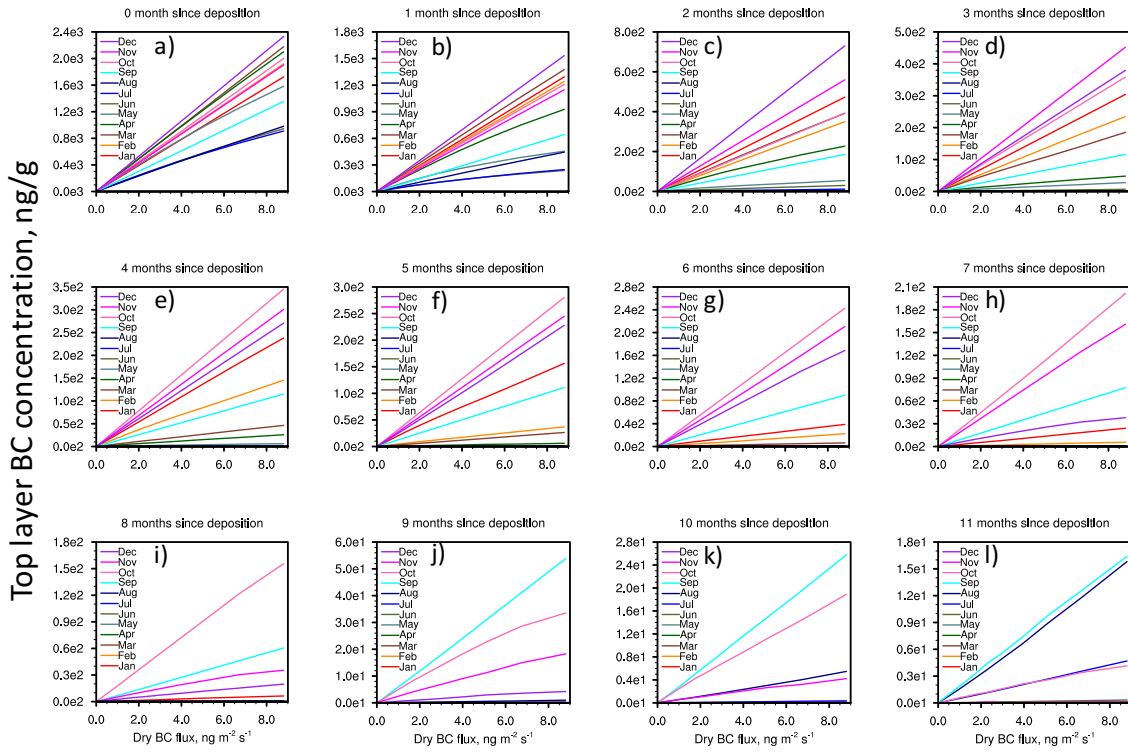
Figure 6. Same as Figure 5, but showing hydrophobic BC concentration in the top

snow layer vs. BC dry deposition flux.

594

595

596

597

598

599
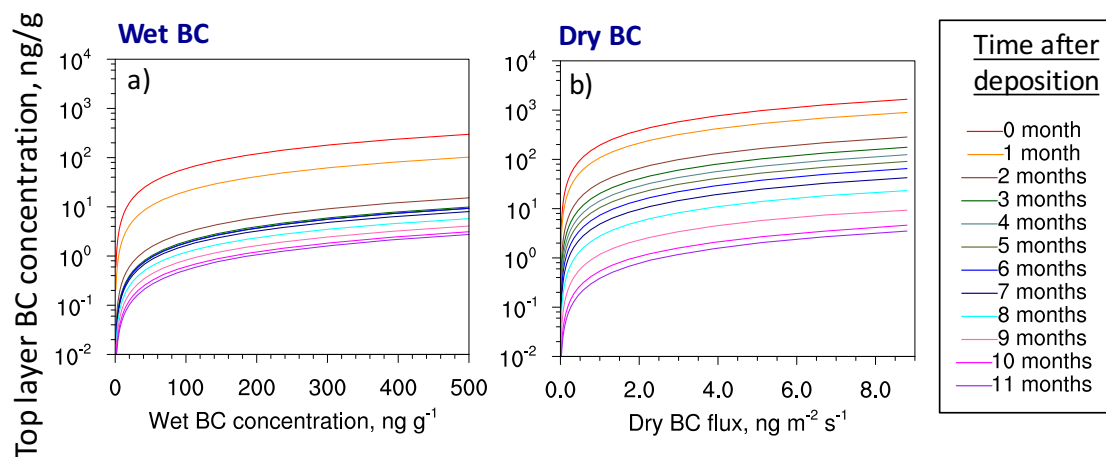
Figure 7. Hydrophilic BC concentration in the top snow layer vs. concentration of BC in precipitation (a), and hydrophobic BC concentration in the top snow layer vs. BC dry deposition flux (b) shown at different times (0-11 months) since deposition. The top-snow layer concentrations are averaged over the Greenland region, over all the deposition months and over ten one-year simulations beginning in years 2006-2015.

607
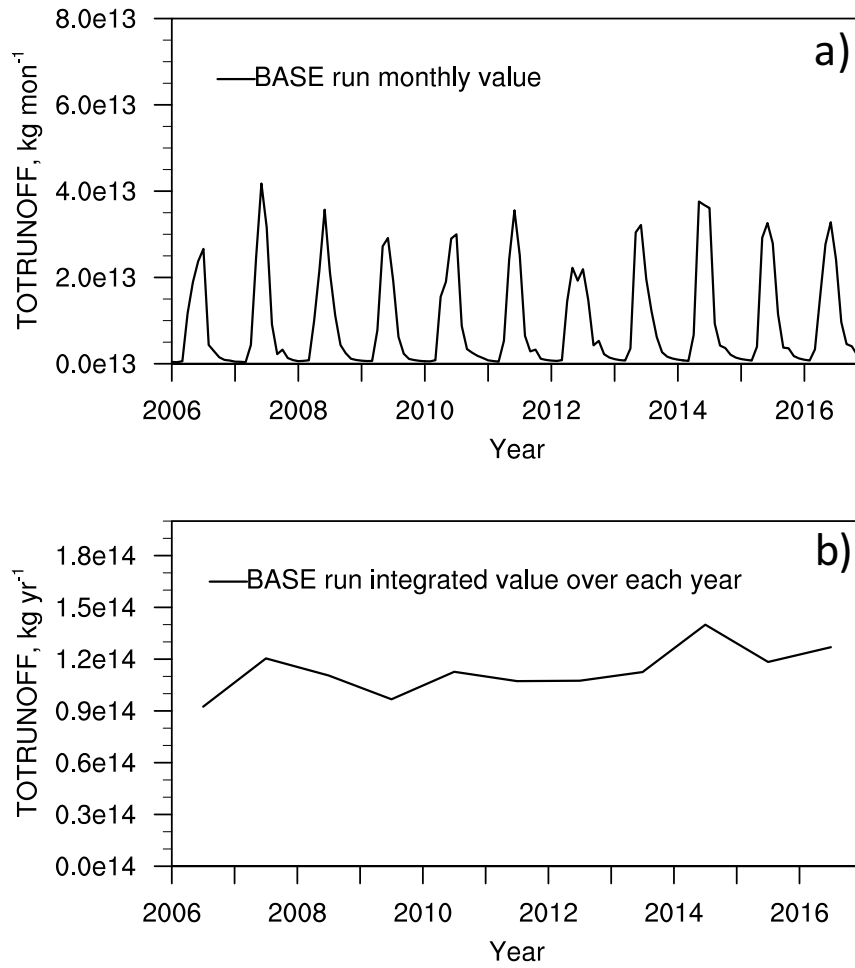
Figure 8. Monthly (a) and annually integrated (b) timeseries of total runoff from

Greenland in the Base run without BC deposition.

610

611
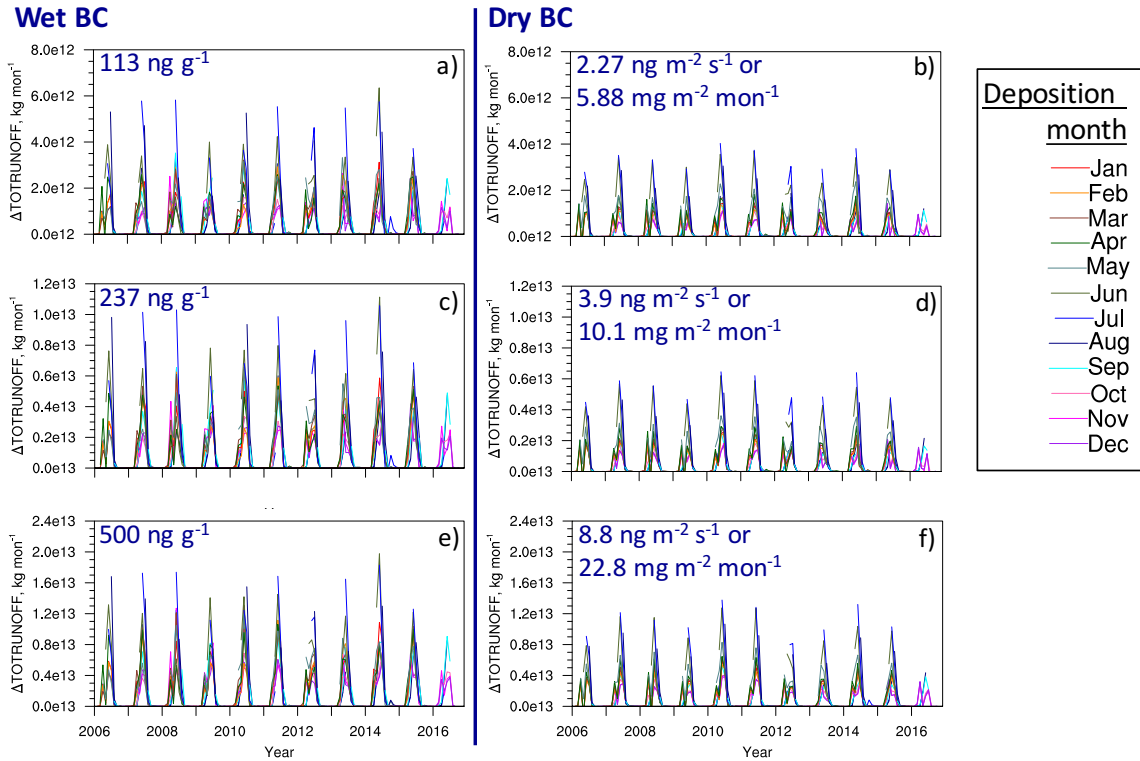
Figure 9. Monthly timeseries of the increase in total Greenland runoff resulting

from BC deposition. Values of BC concentrations in precipitation (a, c, e) and dry

deposition fluxes (b, d, f) are shown in each plot. Each line starts from the BC

deposition month and extends one year. Different line colors represent different

deposition months.

617

618
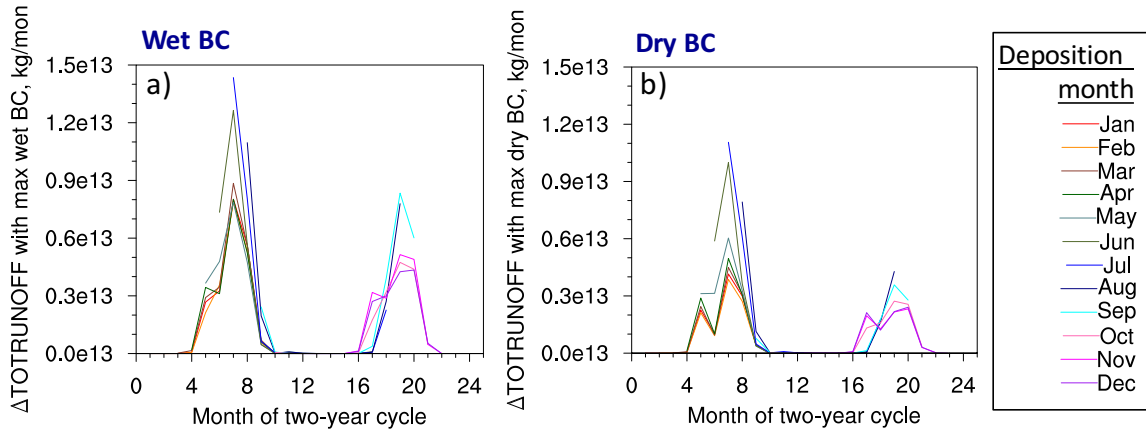
Figure 10. Temporal evolution of ten-year (2006-2015) averaged total runoff

increase resulting from BC deposition, summed over the entire Greenland region

from the simulations with the maximum wet (a) and dry (b) BC deposition. Each line

starts from the BC deposition month and extends one year.

623

**10-year average of 12-month integrated ΔTOTRUNOFF since deposition in Jun**

624
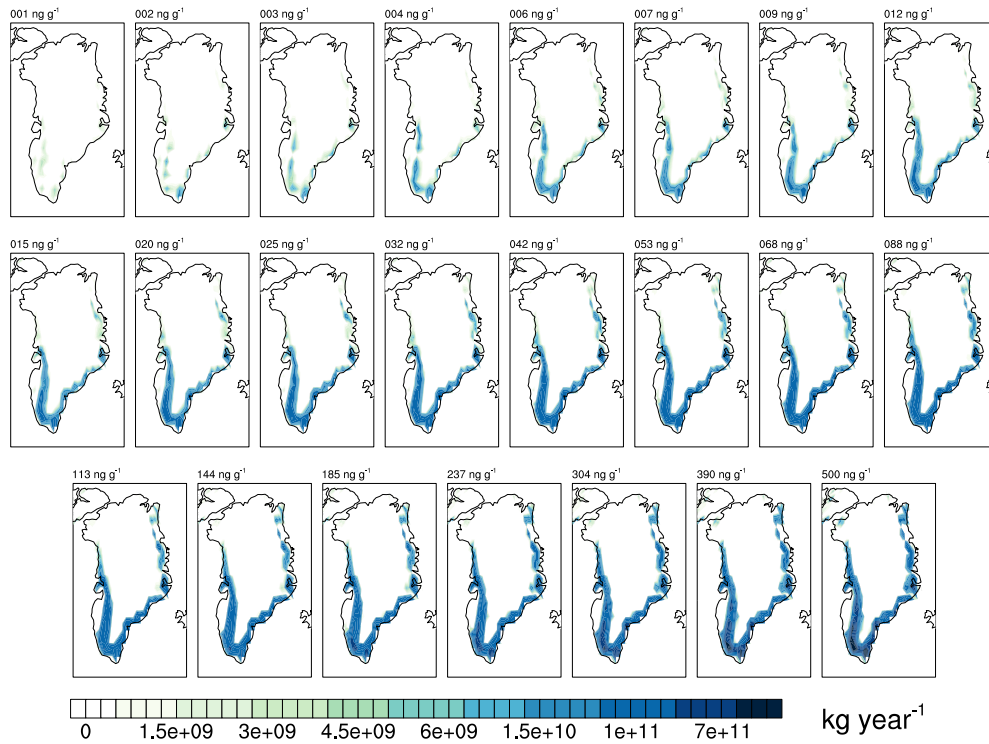
Figure 11. Ten-year average of annually-integrated total runoff increase resulting

from different concentrations of BC in precipitation, deposited only during June.

The average is over ten one-year simulations starting in each year from 2006-2015.

628

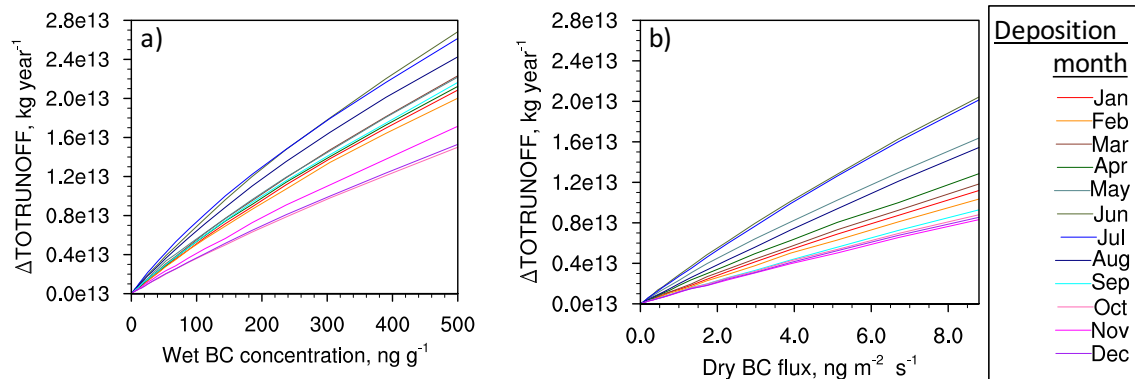10-year average of 12-month integrated ΔTOTRUNOFF since deposition in Jun
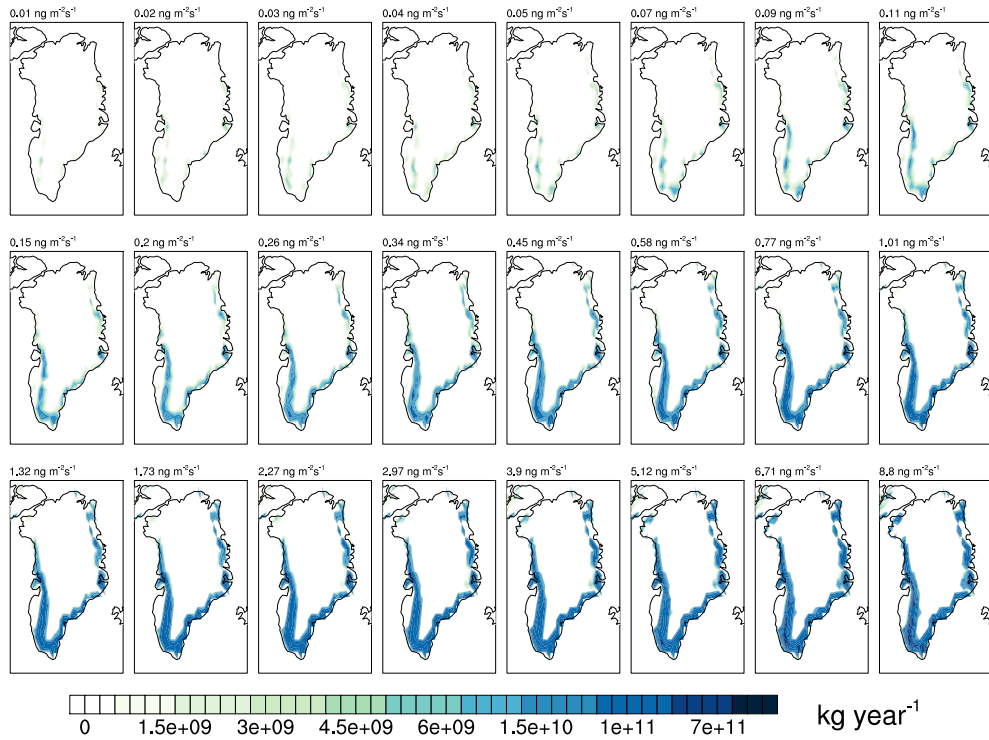
629

630   **Figure 12.** Same as Figure 11, but resulting from different dry deposition fluxes of

631   BC in June.

632

633

634

635

Figure 13. Increase in total Greenland runoff resulting from BC deposition

integrated over one year starting from the month of BC deposition vs. concentration

of BC in precipitation (a) and vs. BC dry deposition flux (b). The runoff values are

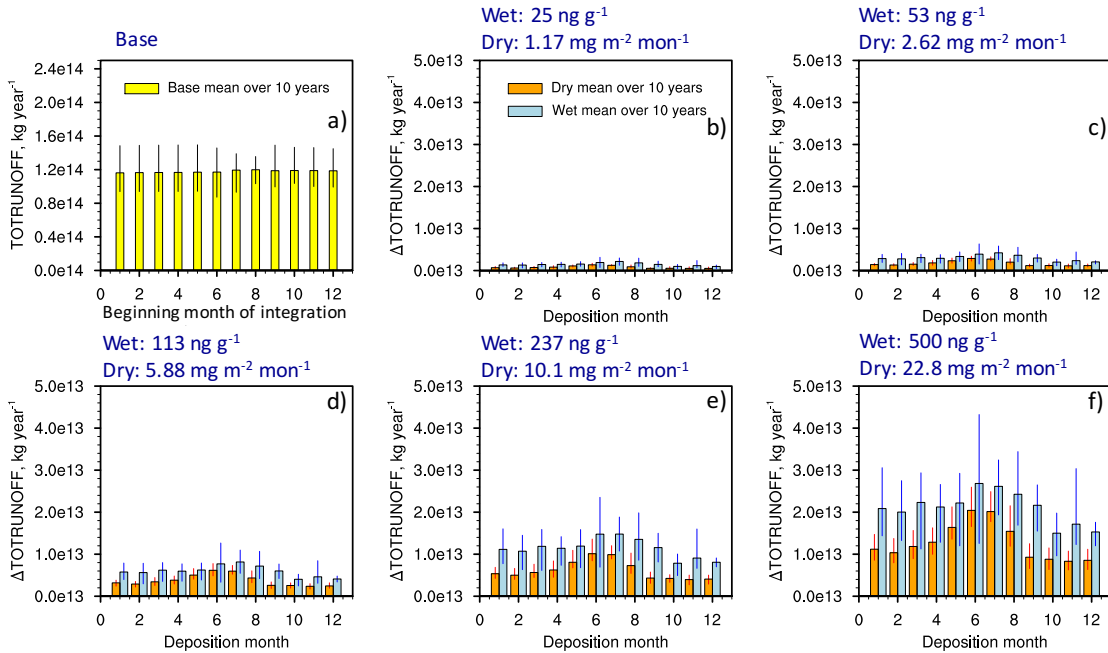summed over the Greenland region and averaged over ten one-year simulations

beginning in years 2006-2015. Different line colors represent different deposition

months.

642

643
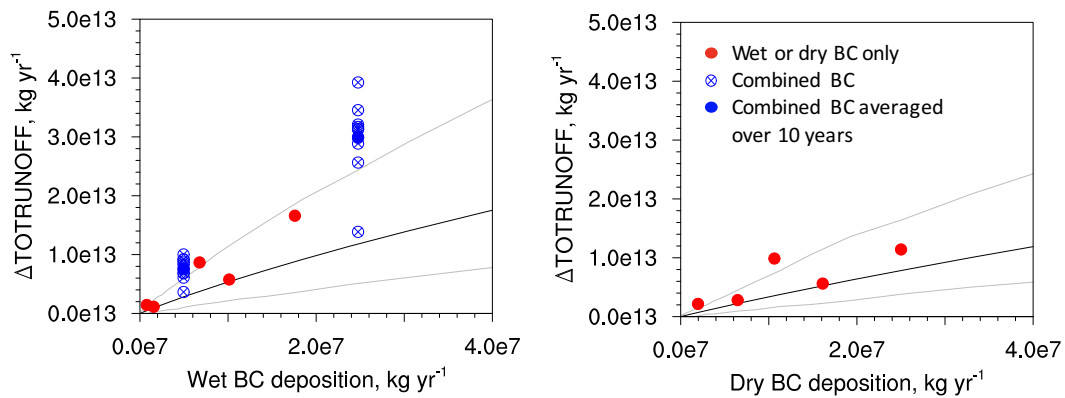
Figure 14. Total runoff in the Base run without BC deposition (a) and the increase in total Greenland runoff resulting from BC deposition (b-f), integrated over one year starting from the month of BC deposition. The bars show mean values and the whiskers depict the full range of values over all ten simulations that each start in a different year from 2005-2016. Values of BC concentrations in precipitation and dry deposition fluxes are shown in the title of each plot (b-f).

652

Figure 15. Increase in total Greenland runoff resulting from BC deposition

integrated over one year starting from the month of BC deposition vs. total wet (a)

and dry (b) BC deposition mass flux over the entire GrIS. The runoff values are

summed over the Greenland region and averaged over all deposition years and

deposition months. Black lines show mean total runoff values, and grey lines show

maximum and minimum values from the entire matrix of simulations. Red dots

represent explicitly-simulated total runoff from the evaluating simulations with

prescribed spatially and temporally-varying wet or dry BC deposition fluxes in

randomly selected months and years. Blue hollow circles represent simulated total

runoff from the evaluating simulations with prescribed combined BC deposition

fluxes integrated over each year of the ten-year simulations. Blue dots show

averages of the hollow circles.

665